Advances in the simulation of debris flow erosion: The case study of the Rio Gere (Italy) event of the 4th August 2017

Tommaso Baggio [a],*, Martin Mergili [b,c], Vincenzo D'Agostino [a]

[a] Department of Land, Environment, Agriculture and Forestry, University of Padua, via dell'Università 16, 35020 Legnaro, PD, Italy
[b] Cascade – Mountain processes and mountain hazards, Institute of Geography and Regional Science, University of Graz, Heinrichstraße 36, 8010 Graz, Austria
[c] Institute of Applied Geology, University of Natural Resources and Life Sciences (BOKU), Peter-Jordan-Straße 82, 1190 Vienna, Austria

ARTICLE INFO

ABSTRACT

Debris flows are natural hazards causing fatalities and damages to infrastructures every year. One of the current challenges is to improve the predictability of such events using simulation tools. In this direction, the paper aims to model debris-flow generation starting from the water component and then simulating the motion of the bulked solid-fluid mixture mass flow. The debris component is progressively increased through entrainment of the channel bed material. The simulation has been performed exploiting the tool r.avaflow, which implements a physically-based model (Pudasaini and Mergili, 2019) for the flow propagation and an empirical multi-phase model for the entrainment processes.

The investigated study case occurred in the Northeastern Alps of Italy, near the town of Cortina d'Ampezzo (Veneto Region), during the summer of 2017. The debris flow was triggered by a heavy rainstorm that caused extreme surface runoff, leading to entrainment of sediment from the channel bed. The debris flow obstructed the bridge of a regional road and consequently flooded the adjacent areas.

Different types of debris flow simulations are performed, testing four specific functions to compute the entrainment rate. The simulated results are then compared against field observations. The analysis considers the differences in volume and depth of entrainment and in the output hydrograph.

We conclude that entrainment is correlated with the terrain slope, particularly if it is calculated on a smoothed digital elevation model, which dilutes a less significant local steepness. We calibrate a spatially distributed slope-dependent erosion coefficient that successfully reproduced the observed entrainment volumes. The outcomes highlight the great importance of simulating debris flow entrainment processes adopting a multiphase model, which resulted particularly suitable for an accurate reproduction of the investigated event. The results, corroborated by further verifications, can improve the reliability of challenging predictive simulations on debris flow erosion.

1. Introduction

Debris flows are gravity-driven mass movements composed of a mixture of water and sediment particles of various sizes (from clay to boulders), moving down through a defined topography (Coussot and Meunier, 1996; Hutter et al., 1994; Jakob et al., 2005; Pudasaini et al., 2005). The motion of such phenomena is influenced by both solid and fluid forces, distinguishing debris flows from related geomorphological processes such as rock avalanches and sediment transport through water floods (Hungr et al., 2014; Iverson, 1997). Debris flows are often characterized by high flow velocities, high impact forces and long runout distances, and represent one of the most hazardous landslide types (Hutter et al., 1996; Jakob et al., 2005; Takahashi and Das, 2014). To predict the necessary parameters for hazard and risk mapping, different simulation tools have been developed in recent years. Most of them are based on single-phase models, in which the solid and fluid phases are considered as a mixture (Bartelt et al., 1999; Grigorian et al., 1967; Iverson, 2012; Sampl and Zwinger, 2004; Savage and Hutter, 1989; Voellmy, 1955), while only a few consider the two components separately (Armanini et al., 2009; Gregoretti et al., 2018; Pitman and Long, 2005; Pudasaini, 2012). Some of these numerical models are implemented in simulation tools and used to map and define hazard areas. Examples of such tools are DAN (Hungr, 1995), FLO-2D (O'Brien et al., 1993), LAHARZ (Iverson et al., 1998), TITAN 2D (Pitman and Long, 2005), SAMOS-AT (Sampl and Zwinger, 2004), RAMMS (Christen et al., 2010), or TRENT–2D (Armanini et al., 2009; Rosatti and Begnudelli, 2013). These simulation tools can mainly reproduce the

propagation through a defined topography of a mass flow starting from a release area (in the case of landslides or avalanches) or alternatively from an input hydrograph (for debris flows or floods).

A current research challenge consists in the reliable simulation of the generation, propagation and deposition of debris flows. Regarding the generation and development of debris flows, threshold conditions in terms both rainfall and runoff amounts are fundamental (Pastorello et al., 2020). Two main processes can be identified, depending on the material characteristics. In poorly-sorted soils where the fraction of silt and clay is higher than 30–40%, debris flows are mainly triggered by shallow landslides in combination with high surface runoff (Baum et al., 2011; Ellen et al., 1982; Kean et al., 2013). In other cases, extreme water flux in a channel can destabilize its bed and banks (Berger et al., 2011) and progressively entrain granular debris, increasing the solid concentration of the flow (Griffiths et al., 1997). The latter process depends on the channel slope, availability of loose material and the exceedance of a water discharge threshold able to exert a certain shear force (Berti and Simoni, 2005; Takahashi, 2000). Moreover, once a debris flow has been triggered it can erode and entrain new debris (Iverson, 2012; Jakob et al., 2005; Reid et al., 2011), increasing its momentum and consequently runout distance and impact force (Iverson et al., 2011; Pudasaini and Fischer, 2020). Bed incision can reach depths of a few metres, or more, leading to a noticeable increase in the transported volume and peak discharge (Berti et al., 1999; Jakob et al., 2005; Pirulli and Pastor, 2012). Particularly if the bed slope increases beyond 10°, the flow can destabilize the channel path (Bagnold, 1966) and sediments can be mobilized and entrained into the flow.

Two types of erosion models have mainly been developed to take in account the increase in destructive potential of the flowing mass: empirical and process-based ones. Empirical laws are easy to use for practical purposes, and they are generally based on an erosion rate, that is time dependent rate of entrained material at the interface between flow and channel bed (Chen et al., 2006; Egashira and Ashida, 1987; McDougall and Hungr, 2005; Takahashi et al., 1992; Takahashi and Kuang, 1986), or on a yield rate (mean entrained volume for channel length unit) (Hungr et al., 1984; Rickenmann et al., 2003). Differently, process-based models consider the physical understanding of exchanges between the flow and the erodible bed (Armanini et al., 2009; Crosta et al., 2015; Fraccarollo and Capart, 2002; Iverson, 2012; Pudasaini and Fischer, 2020). In spite of that, the simulation of debris flow erosion processes still remains a challenge due to the spatial variation of the entrainable material, complex dynamics of such flows and their rheology at the interface layer (Pudasaini and Fischer, 2020). Even if erosion processes are not completely physically understood they should be considered in debris flow simulations, since they noticeably increase the magnitude, runout distance, and impact force of such gravitational flows (Berger et al., 2011; Han et al., 2015; Rickenmann, 2007; Takahashi et al., 1992). Moreover, erosion models should account for the biphasic nature of debris flows, in order to simulate debris flow propagation in the most reliable way (Pudasaini and Fischer, 2020).

The computational tool r.avaflow (Mergili et al., 2017) includes an enhanced version of the Pudasaini and Mergili (2019) multi-phase model and an empirical full multi-phase erosion model. Thanks to these characteristics, r.avaflow is a simulation tool potentially suitable to reproduce the generation of a debris flow event through progressive channel erosion starting from water flux. Although the process-based, fully mechanical multi-phase erosion model presented by Pudasaini and Fischer (2020) could possibly better represent the physics of erosion and entrainment phenomena, for simplicity here we only consider an empirical erosion rate model. Furthermore, it also has the advantage of a more flexible calibration as to a real case study.

In this paper we evaluate the applicability of the simulation tool r. avaflow to reproduce the generation of debris flow event that occurred in 2017 in the Gere catchment, located near the town of Cortina d'Ampezzo (Veneto, Italy). In detail, we test different ways to set up the empirical modelling of erosion implemented in r.avaflow, varying

the coefficient of erosion as a function of the terrain slope. We also calibrate a function to calculate the erosion coefficient as an input map for the simulation tool r.avaflow, based on the erosion observations of the 2017 Gere event. Moreover, we evaluate this new model erosion setup against the default method that fixes the erosion coefficient through the whole computational area. Lastly, we compare the different simulation results, analysing the entrained volume and the output hydrograph.

2. Study area and debris flow event

The analysed event occurred in summer 2017, near the town of Cortina d'Ampezzo located in the province of Belluno (Italy). During the night between the 4th and 5th August 2017, a heavy rainstorm event hit the Bigontina catchment, producing a large amount of surface runoff, consequently triggering a debris flow and intense bed load transport, leading to one fatality and flooding the village of Alverà.

The Bigontina catchment has a surface of 17.5 km^2 extending from 3221 m a.s.l. (summit of Cristallo peak) to 1150 m a.s.l. at the confluence with the Boite river near Cortina d'Ampezzo (Fig. 1). Rio Gere, the alpine stream that produced the debris flow event under investigation, is located in the upper part of the catchment. The Rio Gere joins the Bigontina channel at an elevation of 1650 m a.s.l., just downstream from the bridge of the regional road connecting Cortina d'Ampezzo with Misurina. After the confluence with the Bigontina channel, the thalweg slope of the channel becomes gentler, but the 2017 event still maintained enough energy and turned in a debris flood event (Church and Jakob, 2020), evident by the debris deposit upstream the village of Alverà.

In this paper we analyse the debris flow event triggered and propagated in the Rio Gere basin (Fig. 1 and Fig. 2). The analysed catchment has an area of 1.68 km^2 and a mean slope of 42°. The main channel is 3276 m long and has a mean slope of 19.9°. The relative Melton number (1.19) is consistently higher than the value of 0.5 identified as the threshold for debris flow-prone catchments in north eastern Italy suggested by D'Agostino (1996), meaning that the Gere basin has the morphological characteristics to produce mature debris flows. The basin can be divided into two morphologically and geologically homogeneous parts. We define the basin part with an elevation above 1921 m a.s.l. (elevation of the input hydrograph, Figs. 1, 0.94 km^2) as the "high Gere" catchment and the remaining part (0.74 km^2), down to the confluence with the Bigontina channel, as the "low Gere" catchment. Both areas are formed by dolomite rocks. The "high Gere" consists of steep slopes and near-vertical walls (mean slope 62.2°). The rock channel network is deeply incised into the bedrock (main channel length 1375 m and mean slope of 25.2°), except for a 400 m channel section located upward the input hydrograph point, where the channel bed and banks are formed by loose sediment. The "low Gere" is less steep (the mean catchment and channel slope are 29.3° and 10.9° respectively) and consists of open slopes as consequence of past weathering breakage processes and glacial debris transport. The channel passes through colluvial deposits and is well defined by banks 2–5 m high for the first 450 m downward the input section. Toward the confluence, the channel path becomes rather diffuse and is characterized by loose debris deposits. This sediment can therefore be quite easily mobilized during intense rainfall events. The mean grain diameter surveyed in the lower part of the Gere channel bed after the reported event is 87.2 mm (range: 3.8–1019 mm) (D'Agostino et al., 2018).

The analysed debris flow event took place during the evening of the 4th August 2017. The rainfall event had a total duration of 3 h characterized by two major peaks. The nearest weather station (Misurina, 3.5 km to the east) recorded a total amount of 110 mm between 10.00 p.m. and 12.00 p.m. of the 4th August with two peaks of 10.8 mm/5 min and 10.5 mm/5 min respectively at 10.10 pm and 11.40 pm (local time). The intense runoff in the Gere catchment
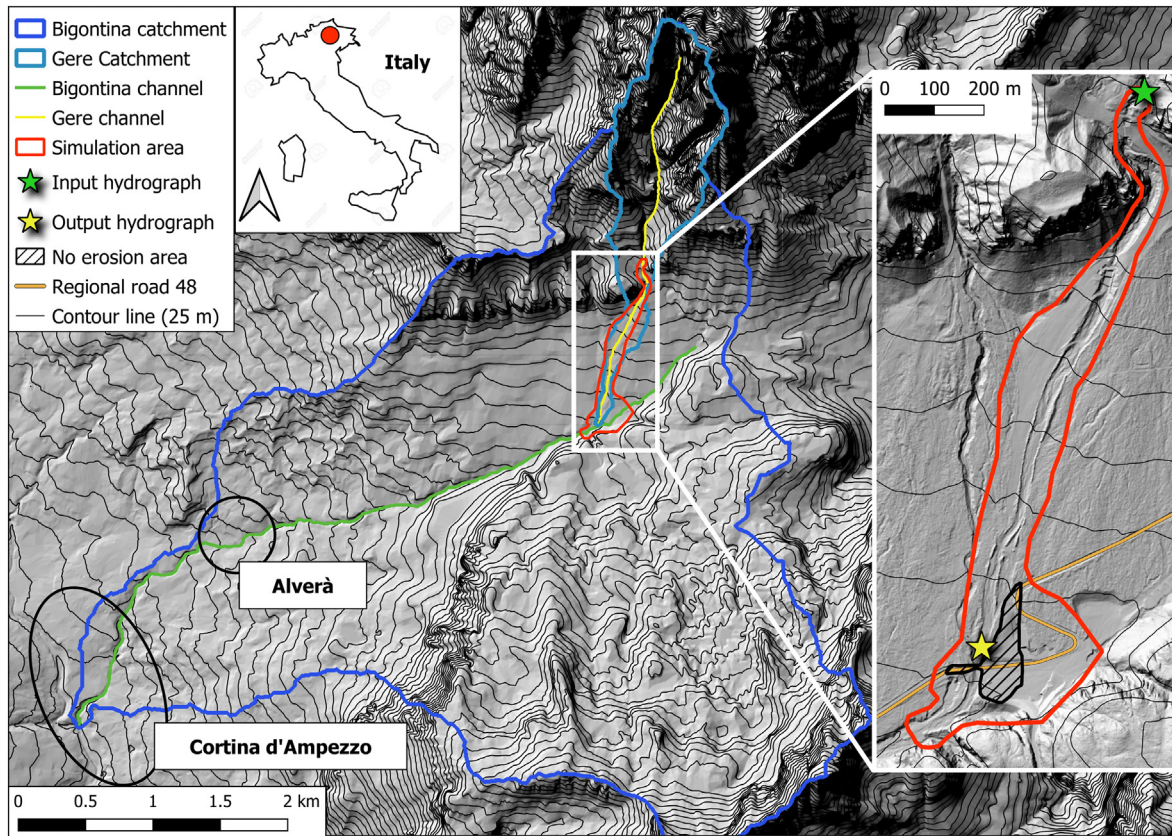
Fig. 1. Overview of the Bigontina catchment (elevation difference between contour lines: 25 m). The no erosion area (black polygon) represents the parking lot, the bridge of the regional road and the chairlift station.

triggered a debris flow through entrainment of debris from the bed and banks.

3. Material and methods

3.1. The simulation tool r.avaflow and the empirical erosion model algorithm

To back-calculate the described event we use the simulation tool r. avaflow, which is able to reproduce rapid mass flows and process chains starting from a defined area down to a deposition zone (Mergili et al., 2017). r.avaflow is a raster module of GRASS GIS 7 (GRASS Development Team, 2020) and is completely open source and freely available at Mergili and Pudasaini (2020). The tool includes two different models: a single-phase shallow water model with Voellmy friction relation (Christen et al., 2010; Fischer et al., 2012) and the Pudasaini and Mergili (2019) multi-phase model with ambient drag (Kattel et al., 2016). The simulation tool is wrapped in Python (data management, pre- and post- processing tasks), while the core of the flow propagation algorithm is implemented in the C programming language. R (R Core Team, 2020) is employed for the validation and visualization functions. The multi-phase mass flow model can simulate the propagation of three different components: solid, fine solid and fluid. Each of them has a specific physical behaviour as described in Pudasaini and Mergili (2019). For this case study we represent the debris as solid component and the water fraction as fluid.

The essential inputs of r.avaflow are a digital terrain model (DTM), the solid and fluid release heights or hydrographs and a set of values describing the flow rheology. Moreover, six specific optional complementary functions are implemented in r.avaflow: conversion of release heights into release depths, diffusion control, surface control, entrainment, stopping and dynamic adaptation of friction parameters.

Focusing on the entrainment model, the algorithm implemented in r.avaflow is based on an empirical multi-phase model. Considering the multi-phase model applied with two phases, the potential fluid and solid entrainment depths ($D_{E,f}$ and $D_{E,s}$ [m]) are expressed as a function of the fluid and solid momentum (M_f and M_s [kg m s^{-1}], fluid/solid mass multiplied by its mean velocity), based on a user-defined empirical erosion coefficient (C_E [kg^{-1}]). The solid fraction ($\alpha_{s,Emax}$) of the entrained material is defined by the user as a fixed number. Alternatively, it can be spatially varied throughout the computational region.

$$D_{E,s} = C_E |M_s + M_f| \alpha_{s,Emax} \Delta t \qquad (1)$$

$$D_{E,f} = C_E |M_s + M_f| (1 - \alpha_{s,Emax}) \Delta t \qquad (2)$$

The solid and fluid entrained depths are added to the flow after each time step and the basal topography (represented by a DTM) is updated at the same time. Flow momenta are updated accordingly. The maximum depth of entrainment can be defined by the user as a raster map.

In this study we use the r.avaflow model (version 2.2), where entrainment is considered as a complementary function of the multiphase model of Pudasaini and Mergili (2019).

To highlight how the erosion model works within r.avaflow, a simple demonstrative debris flow scenario is reproduced. Eleven simulations are performed reproducing a hypothetical debris flow, propagating on a computer-generated hillslope. The topography is represented by a uniform slope, 500 m long with a grade of 0.20 m/m; the channel has a width of 20 m and is delimited by two levees 5 m high. The input hydrograph has a triangular shape, starting with a discharge of 20 m^3/s, reaching a peak of 100 m^3/s after 160 s, decreasing to 20 m^3/s and stopping after 320 s. The input solid volumetric concentration is set to a constant value of 0.5; the total input volume amounts to 19,240 m^3. The eleven simulations are performed on this scenario,
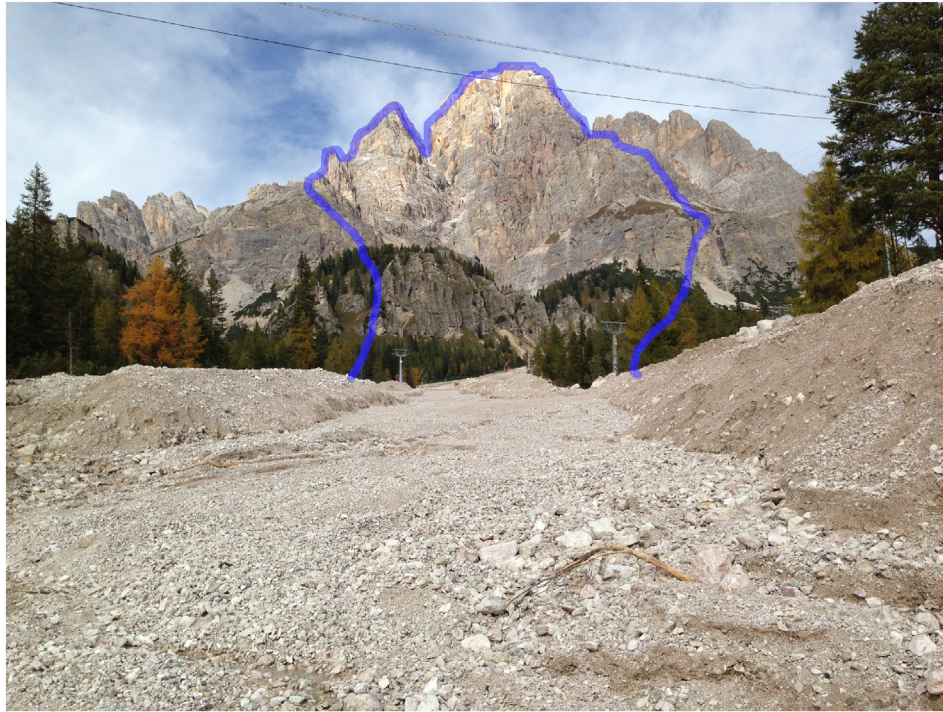
Fig. 2. Photo of the Gere catchment, captured 200 m upward from the confluence with the Bigontina channel toward the watershed border. The blue line represents the watershed line. Photo taken by Francesco Bettella (University of Padova) on 10th April 2017.

progressively varying the erosion coefficient in a range between $5 \cdot 10^{-8}$ and $2 \cdot 10^{-6}$ kg^{-1}. The simulated entrained volumes are then normalized for the channel length and width (eroded volume per unit of channel width and per unit of channel length), obtaining a normalized mean erosion depth (De_n) that is reported in Fig. 3. De_n has a power trend approximated by Eq. (3).

$$De_n = 2.51 \cdot 10^7 \cdot C_E^{1.26} \tag{3}$$

From this scenario it is possible to detect that entrainment is significant ($De_n > 0.15$ m) for values of C_E greater than $3 \cdot 10^{-7}$ kg^{-1}; the upper C_E limit could be detected between 2 and $3 \cdot 10^{-6}$ kg^{-1} corresponding to a mean De_n of 1.6–2.8 m.

3.2. Topographic information and simulation input data

To perform a debris flow simulation with entrainment in r.avaflow, the following data have to be set up as input: DTM, input hydrograph, flow and entrainment parameters. Moreover, to assess the performance of the simulation model we use a post-event LiDAR based DTM.

The pre-event DTM is derived from a LiDAR survey performed in 2009. It has a spatial resolution of 1 m. The point cloud was produced within the PST-A programme (extraordinary Italian plan of remote sensing). We obtained the already processed raster-based DTM from the Italian Environmental Ministry. The vertical and planimetric errors are 0.15 and 0.30 m respectively. The DTM is successively resampled to a resolution of 2 m, using a mean value method, in order to reduce the computational time. The DTM is also modified to represent the obstructed bridge on the regional road SR48. We consider the bridge as a filter of an open check dam for sediment retention, for which the quasi-total trapping condition occurs when $B_{min}/D_{DF} < (1.5-2)$, where B_{min} is the minimum filter dimension (vertical or horizontal dimension) and D_{DF} the maximum boulder diameter of the debris flow (D'Agostino, 2010). In this case B_{min} and D_{DF} are 1.60 and 1.01 m, leading to a complete obstruction of the opening. For this reason, the cells representing

the river bed in the location of the bridge are raised to the elevation of the road.

After the debris flow the whole area of the Bigontina catchment was surveyed through a LiDAR campaign on 26th October 2017. The vertical accuracy is 0.051 m (root mean square error of seven ground control points surveyed with a RTK-GPS) and the mean point density is 10 pts./m^2. From the LiDAR data, the DTM (1 m resolution) is computed using a kriging method (Oliver and Webster, 1990), representing the post-event conditions. Thanks to the availability of the pre- and post-event DTMs we compute the DEM of Difference (DoD). We adopt a simple minimum level of detection approach (Brasington et al., 2000; Fuller et al., 2003), assuming a uniformly distributed error. Difference values lower than the minimum level of detection are not considered in the DoD analysis. The individual errors in the DTMs are propagated in the DoD as the root of the square DTMs' error sum (Brasington et al., 2003).

The resulting area of interest for the simulations is shown in Fig. 1. The computational domain has an extent of 0.183 km^2 corresponding to 44,700 computational cells. The length of the simulated channel is 1483 m with a vertical height drop of 266 m (from 1920 m a.s.l. to 1654 m a.s.l.). The mean channel slope is 10.2°, varying along the channel path: the upper part (the first 500 m downstream from the input hydrograph) has a mean slope equal to 13.6° while the rest of the path has a mean slope of 8.3°.

The position of the input hydrograph is shown in Fig. 1. It is placed in that location in order to simulate the observed erosion process which occurred downstream. The liquid discharge is calculated from the radar measurement of the precipitation in the "high Gere" catchment. The data were acquired by the meteorological station at Monte Macaion (province of Trento, IT), at a distance of 75.5 km from catchment in W direction. The original reflectivity volume scans are elaborated using correction algorithms able to diminish the impact of errors due to (i) radar hardware mis-calibration (Marra et al., 2014), (ii) partial beam blockage (Pellarin et al., 2002), and (iii) signal attenuation due to heavy rain (Marra and Morin, 2018, 2015). Radar reflectivity (R) is converted to rain intensity (Z) following a power-law relationship in
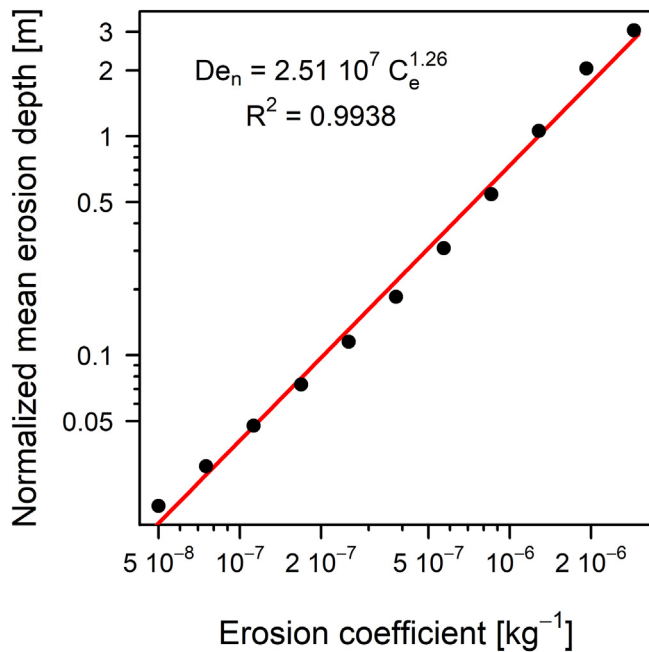
Fig. 3. Results of the sensitivity analysis of the normalized mean erosion depth to the erosion coefficient. The x and y axes are displayed in logarithmic scale.

the form $Z = 308 \cdot R^{1.5}$, well suited for convective precipitation in the area (Anagnostou et al., 2010), and projected to a 1 km grid. Finally, radar estimates are compared with in-situ rain gauge measurements from 3 stations, and adjusted to remove the residual mean field bias (Marra et al., 2014).

After the rainfall assessment, the FLO-2D (O'Brien et al., 1993) two-dimensional flood routing model is used to calculate the fluid hydrograph at the starting location. The SCS - CN (Soil Conservation Service - Curve Number) (Mishra and Singh, 2003) method is adopted to compute the surface rainfall runoff generation together with the model equations for flow propagation as reported in O'Brien (1986). The input data are (i) the DTM (cell size of 20 m); (ii) the initial abstraction (considered equal to 5% of the potential maximum retention); (iii) the Curve Number CN (we used CN at the Antecedent Moisture Conditions AMC III, since the soil was already wet before the event) derived from the combination of the land use-land cover and the hydrological soil group map; (iv) the Manning's surface roughness derived from the land cover map; (v) the radar derived precipitation rainfall intensity (temporal resolution of 5 min and cell size of 20 m, resampled with the natural neighbour algorithm from the 1 km resolution grid). We used an average on the weighted area to derive the CN III and the Manning values, that resulted equal to 75.3 and 0.053 respectively (the lithological, land cover maps and tables used to calculate the CN value and the Manning number are reported in D'Agostino et al., 2018). The model calculates two major discharge peaks of 14.48 and 13.02 m³/s; according to this simulation the time between the two peaks is 64 min (D'Agostino et al., 2018). Since it is not possible to validate the modelled peak water discharge in the field, due to the bedrock channel morphology, we compare it with (i) the empirical relation of Forti (1920) for extreme events and (ii) the rational method (suitable for small alpine catchments (Grimaldi and Petroselli, 2015). The first method results in a peak discharge of 13.07 m³ s⁻¹, while using the rational method we derive a peak of 15.80 m³ s⁻¹. We adopt here a runoff coefficient equal to 0.8 (Berti et al., 1999) and use a concentration time of 27 min coupled with the corresponding mean rainfall intensity of 75 mm/h (according to the above mentioned rainfall data). Through these crossed verifications, we confirm the peak discharge value of the spatially distributed model. The time period between the two major peaks is then cut from the final hydrograph to decrease the computational time, keeping the

fluid flow discharge to 3 m³/s for 300 s (interval: 1100–1400 s). Furthermore, 10% of solid content is added to the input hydrograph to reproduce the flux coming from the upper catchment in a more realistic way. The upper part of the Gere catchment stores a consistent amount of debris (particle diameter range: 25–100 mm) easily entrainable in the case of an intense rainfall event such as the one investigated. Consequently, it is very likely that the flux at the input hydrograph section already transported a certain quantity of solid particles before the debris flow triggering. The resulting input hydrograph used in the simulations is shown in Fig. 4.

The solid and fluid physical parameters used in this case study are shown in Table 1. A description of the parameters is reported in Pudasaini and Mergili (2019). The values are not optimized ad hoc for this event because instruments to detect flow depth and velocity are not present along the channel path and cross sections of the path are strongly modified by the passage of the debris flow causing deep erosion and making a reconstruction of the frontal flow depth unreliable. The physical parameters are basically derived from the back calculation of the 2013 Gadria debris flow event (Bolzano, IT) reported in Baggio (2018), in which an accurate calibration procedure was adopted thanks to the availability of real time event flow depth measurements and relative velocities. The parameters differ from the Gadria case in terms of the basal friction angle (δ) and fluid friction coefficient (C_{FF}). These two parameters are slightly modified in order to obtain reliable front flow velocities as observed in other debris flow events that occurred in catchments of the Dolomites (Berti et al., 1999).

3.3. Observed entrainment

We analyse the erosion depth of each pixel and correlate it with the slope map to verify whether entrainment would depend on the local slope and to obtain a possible correlation between these two variables, and a slope threshold for entrainment. The analysis is performed at the post-event DTM resolution (1 m), dividing the main channel in different reaches 20 m long in order to obtain mean erosion and slope values for each specific channel reach.

Another important use of the DoD is to assess the accuracy of the simulated entrained volumes and entrainment patterns. We investigate the difference between the observed and simulated entrainment patterns. For the whole computational area, we calculate the total eroded volumes and compare them with the simulated ones.

3.4. Improvement of the erosion input data

The empirical erosion algorithm implemented in r.avaflow (Eqs. (1) and (2)) is based on the erosion coefficient that can be set up in the
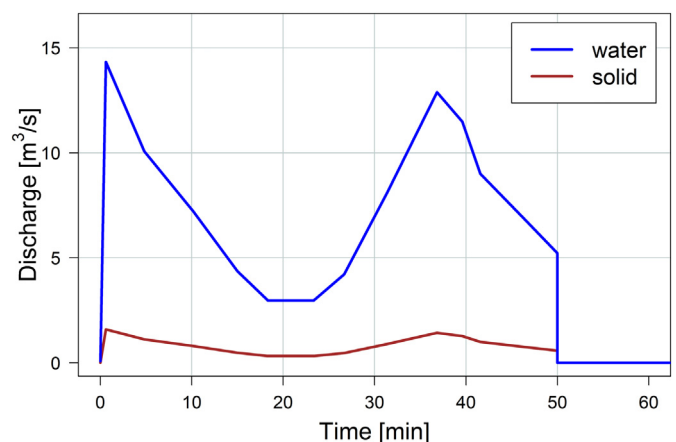

Fig. 4. Input hydrograph used in the r.avaflow simulations (source: D'Agostino et al., 2018).

Table 1

Physical parameters used to perform the simulation in r.avaflow.

Symbol	Physical parameter	Unit	Value
ρ_s	Solid material density	kg m^{-3}	2650
ρ_f	Fluid material density	kg m^{-3}	1000
φ	Solid internal friction angle	Degree	35
δ	Solid basal friction angle	Degree	18
ν	Fluid kinematic viscosity	m^2 s^{-1}	10^{-3}
τY	Fluid yield strength	Pa	0
C_{AD}	Ambient drag coefficient	–	0.02
C_{FF}	Fluid friction coefficient	–	0.05

model as a fixed value or a raster map, allowing a pattern of different entrainment rates within the computational region to be created. Together with the erosion coefficient, the model requires the maximum possible height of erosion and the solid fraction of the entrainable material. For the reported event, we fix the maximum erosion height at 8 m, based on the DTM of difference that highlights a maximum erosion height around 8 m (Fig. 7). In some areas, entrainment is not allowed, corresponding to artificial surfaces (Fig. 1), representing the regional road, the bridge, the parking area and a chairlift station. We set the solid fraction of the entrainable material to 0.7, considering the saturated soil condition caused by the rainfall preceding the debris flow event.

We test the hypothesis that the erosion coefficient can be calibrated as a function of topographic variables. In the literature the variable that mainly affects the erosion rate is the slope (Jakob et al., 2005; Kronfellner-Kraus, 1984; Rickenmann et al., 2003). In this way we use the observed erosion depths in order to calibrate a function able to link the slope with the input erosion coefficient. We study four different functions to derive the spatial distributed erosion coefficient. The types of functions are exponential, linear, logarithmic and power. In particular, the exponential function allows the prediction of a broad variety of eroded volumes for channel units with different terrain slopes, depending on the chosen parameters. Therefore, we test a total of six exponential functions. The tested functions are summarized in Table 2 and shown in Fig. 5. Moreover, we perform a simulation with a fixed coefficient of erosion for the whole computational region ($C_E = 10^{-6.3}$). The function parameters are selected through preliminary 'best-fitting' simulations in which those parameters are progressively varied. 'Best-fitting' depends on the results of the sensitivity analysis introduced along with the entrainment model. The minimum C_E value, for a slope of 0%, is in the range between $2 \cdot 10^{-8}$ and 10^{-7} kg^{-1}. The maximum value of C_E is fixed at 10^{-6} kg^{-1} which, from Eq. (3), leads to a normalized mean erosion depth of 1 m.

In this study, we report the 'best' simulations for the following function types: linear, logarithm and power, while all the performed

simulations are reported for the exponential function. The slope map to calculate the erosion coefficient is derived from the pre-event DTM. As highlighted in the results of the DoD analysis, we avoid the effect of microtopography, re-sampling the slope map derived from the 1 m pre-event DTM to a raster cell size of 10 m and then interpolate it to a final resolution of 2 m, using a bicubic method. This final raster map is used to create the different erosion coefficient maps used in the simulations. To find out which equation better represents the observed entrainment pattern we compare the simulated eroded volumes with the DoD as described in the section 'Observed erosion'. A given simulation is considered accurate if it reproduces the eroded volume within an error of 20% with respect to the observed erosion (derived from the DoD).

Quantification of the increase in debris flow volume and solid concentration due to entrainment is based on the analysis of the simulated output hydrograph located at the lower end of the computational area (the location of the hydrograph is shown in Fig. 1). At the end, we compare the output hydrographs of those five simulations providing the best performance for each type of erosive map (fixed, linear, power, logarithm, exponential). In this way, we analyse the evolution of the solid concentration at the lower end of the computational domain as well as the related peak discharge. We compare the output hydrographs of the ten different simulations performed with different erosion coefficient maps. In this way we can detect whether the differences in the erosion coefficient map lead to a significant difference between the simulated output hydrographs.

4. Results

Firstly, we analyse the patterns of the DoD (propagated error 0.16 m). Fig. 6 (A) illustrates the erosion depths within the computational area. The post-event DTM was recorded on 26th October 2017, 3 months after the investigated event. As shown in Fig. 6 (A), we manage to compute the observed eroded volumes only for two areas (control areas 1 and 2) of the simulated channel path. This is because the material was immediately moved by human activity after the event and before the LiDAR survey. Some places were filled in, others excavated, in order to restore the channel flow and the ski slope for the coming winter season.

The first investigated area is located in the upper part of the computational area (Figure 6 (A), Control area 1) and corresponds to the right turn of the channel. There, major erosion processes due to bank and bed debris entrainment are observed. The maximum values of erosion depth are in the range between 6 and 7 m. In that reach, the main channel has a total length of 216 m and mean slope of 12.9°. Regarding this control area, the calculated total eroded volume is 17,684 m, corresponding to an erosion of 81 m^3 per meter of channel length. The value is so high due to the collapse of part of the external bank in correspondence to

Table 2

Comparison between the simulation results with different coefficients of erosion, calculated for the whole computational area (AOI), the upper part (control area 1) and lower part (control area 2) of the channel path. Observed values are shown as reference.

	C_E	AOI Volume [m^3]	Control area 1 Volume [m^3]	Simulated/observed	Volume/channel length [m^3/m]	Control area 2 Volume [m^3]	Simulated/observed	Volume/channel length [m^3/m]
Observed (DoD)	–	–	10,714 ± 824	–	49.6 ± 3.8	13,215 ± 1625	–	31.2 ± 3.8
Fixed C$_E$ (F)	$C_E = 10^{-6.3}$	73,722	5528	0.52	25.6	21,410	1.66	50.5
Exponential 1 (E1)	$C_E = 10^{(0.05\,S - 7.5)}$	41,702	11,445	1.07	53.0	6570	0.51	15.5
Exponential 2 (E2)	$C_E = 10^{(0.025\,S - 7)}$	29,968	6429	0.60	29.8	5875	0.45	13.9
Exponential 3 (E3)	$C_E = 10^{(0.03\,S - 7.5)}$	10,000	3611	0.34	16.7	1424	0.11	3.4
Exponential 4 (E4)	$C_E = 10^{(0.05\,S - 7)}$	151,393	12,505	1.17	57.9	48,475	3.75	114.4
Exponential 5 (E5)	$C_E = 10^{(0.025\,S - 6.75)}$	83,267	11,601	1.08	53.7	21,815	1.69	51.5
Exponential 6 (E6)	$C_E = 10^{(0.02\,S - 6.75)}$	52,710	8645	0.81	40.0	12,294	0.95	29.0
Linear (LIN)	$C_E = 2.5\,10^{-8}\,S + 10^{-7.5}$	69,947	9659	0.90	44.7	17,932	1.39	42.3
Logarithm (LOG)	$C_E = 4.5\,10^{-7}\ln(S + 5) + 7\,10^{-7}$	128,648	11,140	1.04	51.6	40,619	3.14	95.9
Power (P)	$C_E = 1.5\,10^{-7}\,S^{0.6} + 2\,10^{-8}$	173,469	12,377	1.16	57.3	54,923	4.25	129.7

Exponential E1: $C_e = 10^{(0.05\,S - 7.5)}$

Exponential E2: $C_e = 10^{(0.025\,S - 7)}$

Exponential E3: $C_e = 10^{(0.03\,S - 7.5)}$

Exponential E4: $C_e = 10^{(0.05\,S - 7)}$

Exponential E5: $C_e = 10^{(0.025\,S - 6.75)}$

Exponential E6: $C_e = 10^{(0.02\,S - 6.75)}$

Linear: $C_e = 2.5 \cdot 10^{-8}\,S + 10^{-7.5}$

Logarithm: $C_e = 4.5 \cdot 10^{-7}\ln(S+5) + 10^{-7}$

Power: $C_e = 1.5 \cdot 10^{-7}\,S^{0.6} + 2 \cdot 10^{-8}$
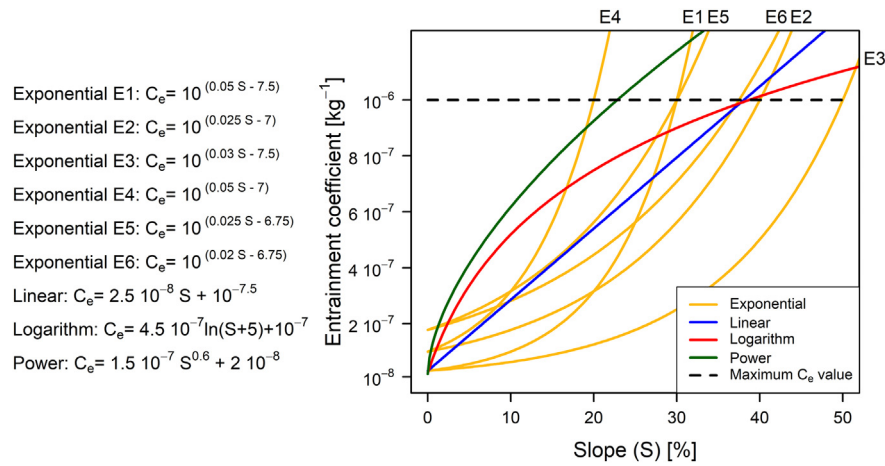
Fig. 5. Functions used to calculate the spatially distributed erosion coefficient in relation to the slope map.

the left turn. The calculated volume of the bank failure is 6,970 m³. Recalculating the erosion per channel meter excluding this volume results in 50 m³/m.

The second control area is located near the confluence with the Bigontina channel (Fig. 6 A, Control area 2). In this part, the channel is not confined to a clearly recognizable path, but flows mainly on the

ski slope. The considered reach has a length of 423 m and a mean slope of 8.9°. The calculated entrained volume caused by the debris flow event is 13,215 m³, corresponding to a volume of 31 m³ per meter of channel length (Table 2).

Regarding the deposit, we make an estimation of the debris volume accumulated at the confluence between the Gere and the Bigontina
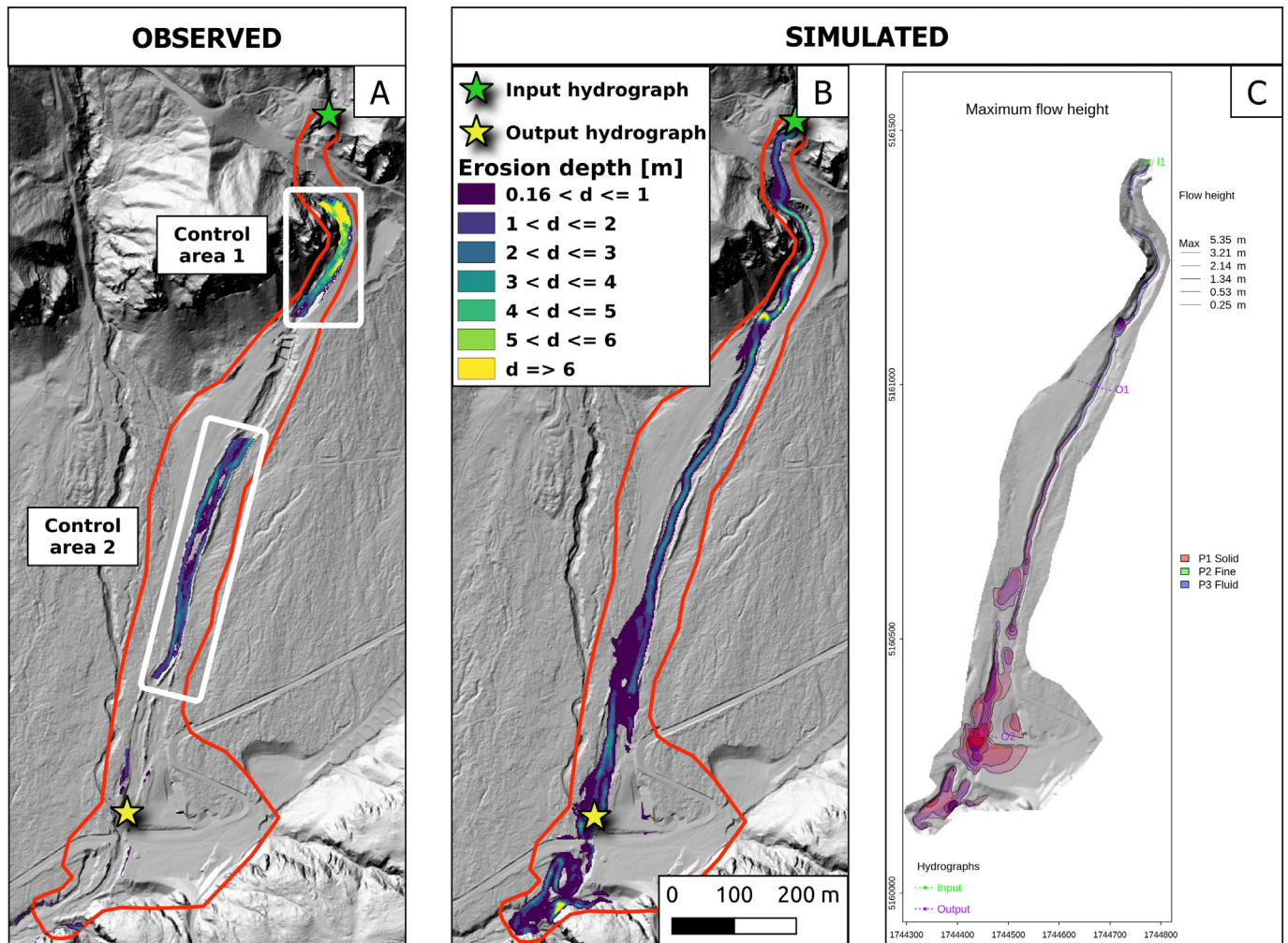

Fig. 6. Maps representing the observed erosion depths (A), simulated erosion depths (B, results of simulation E6) and maximum flow height for simulation E6 (C). In (C) the eroded material is part of the flow height (values lower than 0.25 m are not displayed).

channels. Unfortunately, the 2017 LiDAR was acquired after the anthropogenic movement of the deposited material in order to re-establish the flow passage and so the post-event DTM is not suitable for the volume calculation. However, thanks to helicopter and citizens pictures captured the day after the event, we can identify the debris deposit height relatively to the channel banks. We then fill up the channel post-event DTM for those segments recognised in the pictures and we calculate a total deposit of 13,500 m³. Such value is just an estimation since it is not derived from a rigorous DoD analysis.

4.1. DOD analysis – pixel scale

Starting from the DoD map (Fig. 6 A), we analyse the erosion depth (*ED*) at pixel level and correlate it with the local slope. In Fig. 7 and Fig. 8 we illustrate the results of this analysis. Fig. 7 A shows the correlation between the slope and erosion depth at pixel level (1 m resolution). In Fig. 7 A we simply plot these two variables: the slope is derived from the post-event DTM. The results are widely scattered and it is not possible to identify a significant relationship between these two variables. When substituting the previous slope values with the slope extracted from the map used to calculate the erosion coefficient values (pre-event DTM resampled to a resolution of 10 m and afterwards interpolated to the final resolution of 1 m, using a bicubic method), it is possible to identify a logarithmic trend between slope and erosion depth (Fig. 7 B). The correlation becomes satisfactory only for slopes steeper than 25%. For slope values around 20% the observed erosion depths appear extremely heterogeneous with several observations of erosion depths between 0 and 3 m.

4.2. DOD analysis – 20 m segments of the channel bed

After the analysis at pixel level we focus on erosion of the channel bed in different reaches. To derive a mean value for different reaches of the channel path, we divide it in segments 20 m long for both selected control areas (Fig. 6 A). For each segment, we extract the mean slope (using the slope map to derive the erosion coefficients) and the mean observed erosion depth. The results are plotted in Fig. 8. On these data, we perform a linear correlation between slope and erosion depth, finding a quite good correlation between these two variables. Furthermore, analysing data reported in Fig. 8 we notice that low values of channel slope (10–22%) are associated again (as for Fig. 7 at pixel scale) to a great heterogeneity in erosion depth with a variance of 2.1 m (range: 0.3–2.4 m).
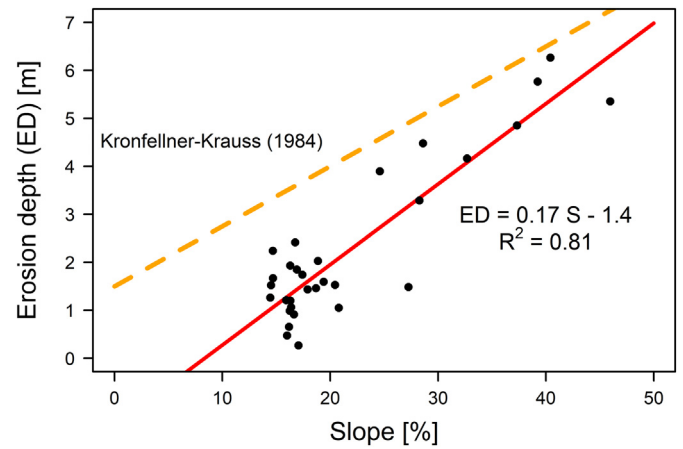
Fig. 8. Analysis of the erosion depths derived from the DOD and local slope. Points represent mean values extracted from the channel bed, dividing it in segments 20 m long. The reported slope values are derived from the pre-event DTM resampled to 10 m and successively interpolated to 1 m (bicubic method). The red line shows the linear regression derived from the points. The orange dashed line represents the maximum erosion depth identified by Kronfellner-Kraus (1984).

Comparing the mean erosion and slope per channel segment with the maximum entrainment thresholds identified by Kronfellner-Kraus (1984), we can confirm that relationship (Fig. 8). Moreover, the Kronfellner-Kraus (1984) threshold and the linear interpolation of the mean segment values show similar trends (0.13 and 0.17, respectively).

4.3. Comparison of observed and simulated volumes

We now focus on the eroded volumes. The simulations performed in this case study are reported in Table 2, together with the results in terms of eroded volumes. The equations employed to obtain the erosion coefficient maps are shown in Fig. 5. In order to assess the accuracy of the simulations, we compare the simulated erosion, represented by the change of the basal surface, and the observed erosion, represented by the DoD. The results are shown in Table 2 and Fig. 6. Looking at the eroded volumes within the computational area, the simulation that entrained the highest debris volume is simulation *P* (*C_E* calculated with the power function) (173,469 m³), while simulation *E3* (*C_E* calculated with the exponential function) predicts the uptake of the least
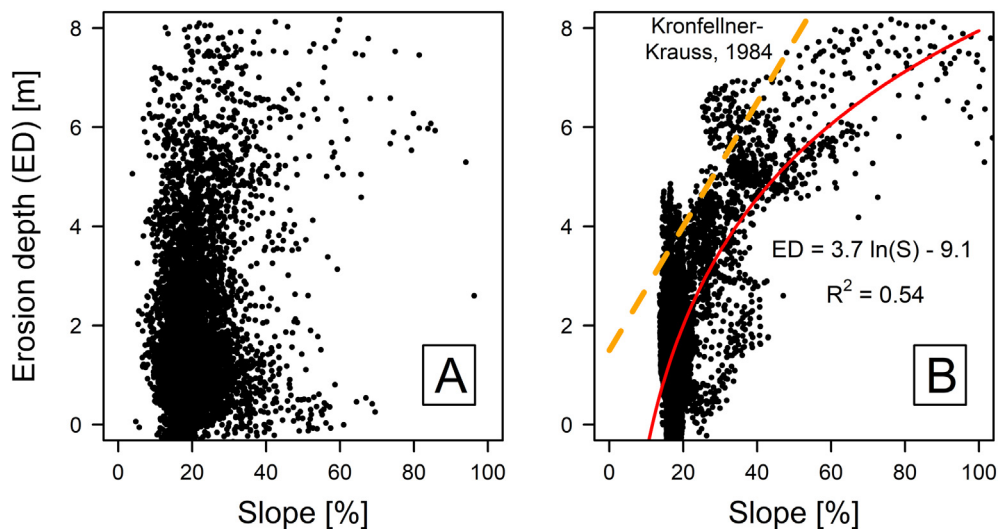
Fig. 7. Analysis of the slope and observed erosion depth derived from the DoD at pixel level. In plot A we extract the slope from the 1 m resolution post event DTM, while in plot B the slope is resampled from the pre-event DTM to 10 m and successively interpolated to 1 m (bicubic method).

amount of material (10,000 m³). Analysing the eroded volumes for the control area 1, most of the simulations (E1, E4, E5, E6, LIN, LOG and P) yield an accurate (error less than 20%) prediction in terms of the eroded volume. The simulations F (fixed C_E), E2 and E3 underestimate the eroded volumes with an error of between 48 and 66% (Table 2). Looking at the control area 2, the simulation that most accurately represents the observed eroded mass is simulation E6 with a difference between the simulated and observed eroded volumes of −614 m³ (relative error of −5%). Simulations F, E4, E5, LIN, LOG and P entrain a large amount of solid material with respect to the observed debris volume (error between 39 and 425%). On the contrary, the simulations E1, E2, E3 entrained considerably small amounts of volume (error between −49 and -89%).

The ratio between the simulated and observed eroded volumes reveals that simulation E6 represents the observed data for both control areas in the most accurate way (Table 2). The other simulations represent either control area 1 or control area 2 in an accurate way. Fig. 6 shows the results of simulation E6 for the entrained depths and maximum flow depths (Fig. 6B and C, respectively).

Analysis of the output hydrograph located just upstream from the confluence with the Bigontina torrent (Fig. 1) allows the simulated peak discharges and solid volume concentrations of the best five simulations to be quantified. The hydrograph showing the discharge and flow volumetric solid concentration for every time step is displayed in Fig. 9 (for the exponential type simulations we only show E6 for clarity). We further detect that all the simulated flows increase their solid content, reaching a steady value around 0.4–0.6 at the output hydrograph location, but they never exceed a value of 0.7. The solid volumetric concentration increases over time for all the simulations represented in Fig. 9 because of the dam effect of the simulated bridge obstruction. The obstruction involves deposition of the solid component while the fluid fraction slowly flows downstream, consequently increasing the volumetric solid concentration at the output hydrograph location (Fig. 9). Looking at the discharge, the performed simulations show two types of patterns. Simulations F, P and LOG show a single discharge peak corresponding with the first surge, while the second surge is not captured in the output hydrograph. On the contrary, simulations LIN and E6 show the opposite pattern with a weaker discharge peak for the first surge and a stronger one for the second surge. This can be explained by the terrain morphology of the computational area and the maximum entrainable depth. The simulations P and LOG entrain a large amount of sediment especially in control area 2 (Table 2), leading to a big discharge peak at the output hydrograph for the first surge. However,

they do not show the same discharge intensity for the second surge because the maximum entrainment depth has almost been reached after the passage of the first surge. In this way, the simulations P and LOG do not predict a large amount of entrainable sediment available for the second surge. On the contrary, the simulations LIN and E6 show higher discharge peaks for the second surge, resulting in agreement with the witnesses to the event. In this case, the first surge is mitigated by the morphology of the computational area in which the obstructed bridge creates a dam effect, decreasing the flow velocity and promoting deposition of the solid component. This mitigation effect is not present with the second surge, because the channel has already been filled up with the sediment of the first surge. The second discharge peak thus results decisively more intense than the first one, also due to remobilisation of the previously deposited debris.

Fig. 9 reveals two further aspects: the first surge is highly impulsive showing a sharp discharge increment, conserving a pattern which is similar to the input hydrograph. In addition, the solid volumetric concentration is similar for all the simulations, looking at the first surge, with values around 0.50–0.55.

5. Discussion

We investigated the debris flow event which occurred in a Dolomitic catchment near the town of Cortina D'Ampezzo (IT) on 4th August 2017. We firstly analysed the observed erosion pattern and then adapted the parameterization of the erosion model implemented in r. avaflow in order to reproduce the observed entrained volumes in the most accurate way. The first analysis was based on the comparison of pre- and post-event DTMs. From these data we identified a maximum erosion depth value of 8 m. Entrainment was comparatively high with a value of 50 m³ per meter of channel unit in control area 1 and 31 m³ per meter channel unit in control area 2. Comparing these values with other erosion amounts in literature, it is possible to highlight the intensity of the event in terms of debris flow erosion. Rickenmann and Zimmermann (1993) reported maximum erosion depths for debris flows in the Swiss Alps of around 5 m. Hungr et al. (2005) reviewed debris flow erosion analysing the entrainment per channel unit, obtaining a range 0–50 m³/m considering more than 500 events reported in 14 studies from different mountain chains. Extreme values of 300 m³/m were identified by Rickenmann and Weber (2003) for debris flow events in Kazakhstan due to bank failure. Regarding the eastern Alps, Marchi and Cavalli (2007) related values of entrainment per channel unit to the cumulative frequency. In the same study they investigated
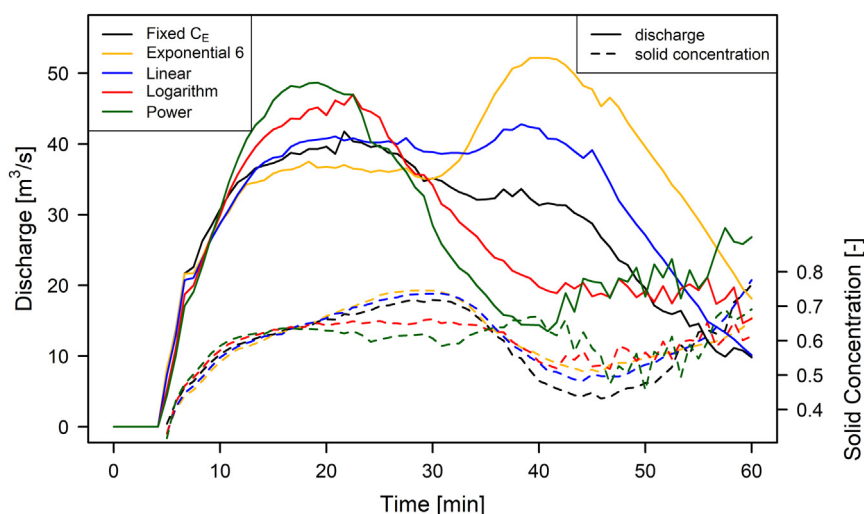

Fig. 9. Output hydrographs (total discharge and volumetric solid concentration over time) of the performed best simulations just upstream of the confluence with the Bigontina torrent (location shown in Fig. 1).

a debris flow event, reporting a maximum value of 110 m³ per meter of channel unit. Furthermore, Marchi and D'Agostino (2004) analysed the magnitude of 127 debris flow events in the Eastern Alps, observing that the erosion per channel unit is rarely larger than 50 m³/m (7% of the entire sample). Thus, according to these findings, the present case study with a maximum value of 50 m³/m is established as one of the most extreme values recorded in the eastern Alps and worldwide.

Such high eroded volumes per channel unit are the result of a combination of different contributing factors. In the investigated area the availability of a thick layer of loose sediment, a well-defined channel path and the saturation conditions enhanced the debris flow propensity to erosion processes in a noticeable way (Berger et al., 2011; Cannon et al., 2003; Reid et al., 2011). Moreover, the rainfall pattern distribution, characterized by two peaks of equal high intensity, constantly stressed the torrent path, leading to a major destabilization of the channel bed.

Another important driver of erosion in channelized beds is the slope (Hungr et al., 2005); therefore we analysed this variable related to the observed erosion depths. We noticed that plotting the erosion depths against slope values at the DTM resolution we obtained no significant relationship, as illustrated in Fig. 7 plot A. Next, we removed the microtopography from the slope map by resampling the slope map from the resolution of 1 m to 10 m (mean value method) and interpolating it to the initial resolution (bicubic method). The new slope values correlated well with erosion depths in a logarithmic way (Fig. 7, plot B). This reveals that debris flow erosion is more related to a smoothed slope than to a more precise slope value analysed in this case at the resolution of a 1 m LiDAR DTM. We may infer that the energy amount of routing debris flows is so big that it can hardly be influenced by small changes in slope, especially if we refer to a resolution of 2 m.

In order to understand the mean erosion rate along the channel path, we divided the torrent bed in reaches of 20 m and then correlated the mean erosion depth with the slope of each bed area. We were able to derive a regression trend line between these two variables confirming the maximum threshold identified in Kronfellner-Kraus (1984), supported by data reported in Rickenmann and Zimmermann (1993). Marchi et al. (2009) computed a similar analysis for a debris flow event in the Eastern Alps (Rio Cucco basin), observing high erosion depths (6–9 m) for channel slopes of 30–40% and lower erosion depths for steeper sections (regarding the loose sediment bed material). We further confirmed the threshold identified by Takahashi (2007) for the initiation of stony debris flows for channel bed erosion equal to a slope value of 25%. In Fig. 8, this value identifies those channel reaches for which erosion processes resulted more intense, with mean erosion depths exceeding 3 m, nevertheless a significant contribution to debris flow triggering cannot be excluded in the range 15–20% (Fig. 8). In our case study, the interpretation of the modelling results also confirmed that slope is one of the main drivers in entrainment processes related to debris flow events in natural confined beds, given that the other torrent conditions remain the same along the path (geology, availability and grain size of loose material and bed width). The slope can be considered as an indicator of the limit strength of the debris to bear erosion for a certain catchment geology. Complementarily, we could suppose that higher is this limit/slope more intense is the erosion when this limit is exceeded, because of great shear stresses become suddenly effective during flashy floods. In addition, after the solid particles detach from the channel bed, the erosion process is amplified by the component of their weight along the direction of the flow momentum (a component that increases as the terrain slope increases). For such reason, we might consider the topographic slope as the main control for debris flow erosion as confirmed in Fig. 7 and Fig. 8. However, more studies for a range of rheological and geological situations are required to further investigate the role of slope angle as a control for debris flow entrainment processes.

Since we identified such slope control in channel erosion processes, then we improved the parameterization of the empirical erosion model implemented in r.avaflow calculating the coefficient of erosion (C_E) as a function of the slope. Four different types of functions were used to calculate C_E. We compared the eroded simulated volumes with the DoD and showed that an appropriately parameterized exponential function represents the erosion pattern in the most accurate way. We compared these results with a simulation performed with a fixed coefficient of erosion equal to $10^{-6.3}$ kg^{-1}. This comparison shows a more accurate simulation using an exponentially slope-dependent erosion coefficient, highlighting empirically adequate results for the two control areas characterized by different mean slopes.

We have deliberately employed a simple and straightforward erosion model, multiplying the momentum of the flow with an empirical entrainment coefficient, and calculate this coefficient according to the slope. In the newer literature, in contrast, erosion is often computed by comparing the mechanical strengths of the flow material and the bed (Iverson and Ouyang, 2015; Pudasaini and Fischer, 2020). Whereas these models have a sound physical basis, they are still very hard to apply to real-world cases in practice. The model outcomes are very sensitive to the difference between the mechanical properties of the flow and the surface – however, these properties are usually unknown, and the best which could be done in this respect would be to calibrate the strength parameters with observations. We have followed the alternative way to define those areas as erodible where the bed material is most likely weaker than the flow material, based on geomorphological evidences, and then tried to quantify erosion by hypothesizing a relationship with flow momentum and topography. However, there is an urgent need for more research on how to appropriately compute and parameterize erosion through debris flow processes.

In this study, we were able to reproduce the generation and dynamic of a debris flow through channel bed entrainment thanks to the use of the Pudasaini and Mergili (2019) multi-phase model included in the simulation tool r.avaflow, employing an empirical multi-phase erosion model applied with two phases (Eqs. (1) and (2)). The r.avaflow tool allows the simulation of different types of mass flows and considers the strong relation between the fluid, fine solid and solid momentum transfer. It could therefore be used to reproduce the interaction, mixing and separation of up to three considered phases. The simulations performed in this study used two phases and showed that the solid and fluid components entrained by the flow were mixed and contributed to the momentum increase of the flowing mass. In particular, the fluid component played the main role in the entrainment process particularly in the initial stage, progressively entraining solid material (the input hydrograph had a 10% solid fraction). At the lower end of the computational area, the results of simulation E6 (C_E as an exponential function of the slope) showed a solid fraction up to 50–55% for the two discharge peaks, typical for a mature debris flow. The similar solid concentration of the performed simulations can be explained by (i) the value of the bed solid fraction (Eqs. (1)–(2), $\alpha_{s,Emax}$) fixed to 0.7 and (ii) the effect of the fluid fraction necessary to produce drag force for solid phase motion. In particular, if the fluid fraction is not sufficient to move the total amount of the solid phase, the solid part tends to deposit and eventually, it can be successively moved if the upcoming flow can generate enough drag force. In this way, the simulated solid fraction at the output hydrograph never exceeded a value of 0.57 during the flow propagation, as shown in Fig. 9 for the first 20 min of the different simulations. Afterwards, the solid component noticeably increased for the deposition process caused by the bridge.

Comparing the simulated and observed entrained volumes and the erosion depths per channel unit for the two control areas we found a good accuracy of the simulated amount of entrained material (Table 2). The peak discharge increased up to four times the input hydrograph for the second surge. The observed and simulated entrainment patterns lead to the consideration that erosion processes have to be accurately assessed for the simulation of debris flows over mobile beds since they can notably increase their destructive potential as highlighted in earlier studies (Berger et al., 2010; Chen and Zhang, 2015; Gregoretti et al., 2019; Mergili et al., 2018; Rosatti and Begnudelli, 2013). In addition, the

proposed entrainment approach could be straightforwardly applied for the simulation of a dam break scenario. The erosion coefficient is really small in the case of flat terrain (C_E is never equal to zero), but if the flow momentum results high, the fluid flux can trigger a debris flood or debris flow depending both on its momentum and terrain topography. The obtained slope-dependent function for C_E assessment is at the same time an easy and efficient approach to model debris flow erosion. The proposed method can be potentially implemented also in other mass flow propagation models, making it a broadly useful approach.

The investigated case study can be classified as extreme considering the observed erosion rates, caused by the availability of a large amount of loose saturated debris. The findings correspond to earlier studies both for the Alps (Marchi and Cavalli, 2007) and worldwide, and the erosion model reported here is considered suitable to reproduce this event. We can affirm that the model may be used to accurately estimate maximum thresholds of erosion in the simulations of debris flows over natural channels. However, the calibrated exponential function to derive the erosion coefficient has to be accurately tested with other case studies to evaluate its reliability. Future refinements of the proposed approach might consider other factors affecting erosion such as bed confinement and bed forms, and parameters describing the debris flow composition in more detail.

6. Conclusions

We investigated the debris flow event which occurred in 2017 in the Bigontina dolomitic catchment of the Eastern Alps in Italy. The event obstructed the bridge of the regional road and successively triggered an intense bed load transport event that flooded the village of Alverà causing one fatality. In this study we focused on the entrainment processes of the debris flow event. The availability of pre- and post-event LiDAR campaigns allowed us to study the spatial patterns of the volumes entrained by the debris flow. We then successfully back-calculated the debris flow using the simulation tool r.avaflow and proposing a new parameterization of the erosion model.

Regarding the observed eroded volumes, we compared the investigated event with studies reported in the literature and we can define this event as one of the most extreme affecting the eastern Alps, in terms of documented erosion. Furthermore, we confirmed that channel erosion is highly correlated with a smoothed slope map (Fig. 7). Moreover, we analysed the mean erosion depth observed within each channel segment (Fig. 8), and we confirmed the threshold suggested by Kronfellner-Kraus (1984).

Regarding the back calculation part, we used the Pudasaini and Mergili (2019) multi-phase model included in r.avaflow, together with the empirical erosion model. Since erosion is related to slope (Fig. 7 and Fig. 8), we evaluated different equations to calculate a spatially distributed erosion coefficient based on the topographic slope (Fig. 5). We compared the simulated eroded volumes against the difference between the pre- and post-event DTMs. Thereby, an exponential function of the slope turned out as the most accurate way to derive the spatially distributed erosion coefficient for simulating the entrainment process and to capture the complex dynamics of a composite/double peak triggering event. Another important simulation result is the generation of a mature debris flow through progressive entrainment of the solid component along the channel path. The input hydrograph is characterized by 10% solid content (Fig. 4), while at the end of the computational area the solid ratio is 45–60% (Fig. 8), noticeably increasing the peak discharge.

This study highlights that channel erosion processes have to be taken into great account in debris flow simulations because they increase destructive potential, times of passage of the surges, and dynamics of the events. Furthermore, r.avaflow appears suitable for the simulation of debris flows on erodible channels thanks to the multiphase propagation model in combination with a multi-phase empirical erosion model. In particular, we defined a new method to improve the

quality of the entrainment parameters by calibrating a function for the calculation of the spatially distributed erosion coefficient. Future studies have to confirm and possibly to improve the reported approach in order to make it suitable for predictive simulations within the framework of hazard mapping and risk management.

Declaration of competing interest

The authors declare that they have no known competing financial interests or personal relationships that could have appeared to influence the work reported in this paper.

References

Anagnostou, M.N., Kalogiros, J., Anagnostou, E.N., Tarolli, M., Papadopoulos, A., Borga, M., 2010. Performance evaluation of high-resolution rainfall estimation by X-band dual-polarization radar for flash flood applications in mountainous basins. J. Hydrol. 394, 4–16. https://doi.org/10.1016/j.jhydrol.2010.06.026.

Armanini, A., Fraccarollo, L., Rosatti, G., 2009. Two-dimensional simulation of debris flows in erodible channels. Comput. Geosci. 35, 993–1006. https://doi.org/10.1016/j.cageo.2007.11.008.

Baggio, T., 2018. Assessment of the Mass Flow Multi- Process Simulation Model: R. Avaflow (Master Dissertation). University of Padova.

Bagnold, R.A., 1966. An Approach to the Sediment Transport Problem from General Physics. USGS Prof. Pap. 42. https://doi.org/10.1017/S0016756800049074.

Bartelt, P., Salm, B., Gruber, U., 1999. Calculating dense-snow avalanche runout using a Voellmy-fluid model with active/passive longitudinal straining. J. Glaciol. 45, 242–254. https://doi.org/10.3189/002214399793377301.

Baum, R.L., Godt, J.W., Coe, J.A., 2011. Assessing susceptibility and timing of shallow landslide and debris flow initiation in the Oregon Coast Range, USA. International Conference on Debris-Flow Hazards Mitigation: Mechanics, Prediction, and Assessment, Proceedings, pp. 825–834 https://doi.org/10.4408/IJEGE.2011-03.B-090.

Berger, C., McArdell, B.W., Fritschi, B., Schlunegger, F., 2010. A novel method for measuring the timing of bed erosion during debris flows and floods. Water Resour. Res. 46, 1–7. https://doi.org/10.1029/2009WR007993.

Berger, C., McArdell, B.W., Schlunegger, F., 2011. Direct measurement of channel erosion by debris flows, Illgraben, Switzerland. J. Geophys. Res. Earth Surf. 116. https://doi.org/10.1029/2010JF001722 (n/a-n/a).

Berti, M., Simoni, A., 2005. Experimental evidences and numerical modelling of debris flow initiated by channel runoff. Landslides 2, 171–182. https://doi.org/10.1007/s10346-005-0062-4.

Berti, M., Genevois, R., Simoni, A., Tecca, P.R., 1999. Field observations of a debris flow event in the Dolomites. Geomorphology 29, 265–274. https://doi.org/10.1016/S0169-555X(99)00018-5.

Brasington, J., Rumsby, B.T., McVey, R.A., 2000. Monitoring and modelling morphological change in a braided gravel-bed river using high resolution GPS-based survey. Earth Surf. Process. Landforms 25, 973–990. https://doi.org/10.1002/1096-9837(200008)25:9<973::AID-ESP111>3.0.CO;2-Y.

Brasington, J., Langham, J., Rumsby, B., 2003. Methodological sensitivity of morphometric estimates of coarse fluvial sediment transport. Geomorphology 53, 299–316. https://doi.org/10.1016/S0169-555X(02)00320-3.

Cannon, Susan H., Cannon, S.H., Gartner, J.E., Parrett, C., Parise, M., 2003. Wildfire-related debris-flow generation through episodic progressive sediment-bulking processes, western USA. Debris-Flow Hazards Mitigation: Mechanics, Prediction, and Assessment.

Chen, H.X., Zhang, L.M., 2015. EDDA 1.0: Integrated simulation of debris flow erosion, deposition and property changes. Geosci. Model Dev. 8, 829–844. https://doi.org/10.5194/gmd-8-829-2015.

Chen, H., Crosta, G.B., Lee, C.F., 2006. Erosional effects on runout of fast landslides, debris flows and avalanches: a numerical investigation. Géotechnique 56, 305–322. https://doi.org/10.1680/geot.2006.56.5.305.

Christen, M., Kowalski, J., Bartelt, P., 2010. RAMMS: numerical simulation of dense snow avalanches in three-dimensional terrain. Cold Reg. Sci. Technol. 63, 1–14. https://doi.org/10.1016/j.coldregions.2010.04.005.

Church, M., Jakob, M., 2020. What is a debris flood? Water Resour. Res. 56. https://doi.org/10.1029/2020WR027144.

Coussot, P., Meunier, M., 1996. Recognition, classification and mechanical description of debris flows. Earth-Science Rev. 40, 209–227. https://doi.org/10.1016/0012-8252(95)00065-8.

Crosta, G.B., De Blasio, F.V., Locatelli, M., Imposimato, S., Roddeman, D., 2015. Landslides falling onto a shallow erodible substrate or water layer: an experimental and numerical approach. IOP Conf. Ser. Earth Environ. Sci. 26, 012004. https://doi.org/10.1088/1755-1315/26/1/012004.

D'Agostino, V., 1996. Analisi quantitativa e qualitativa del transporto solido torrentizio nei bacini montani del Trentino Orientale. 1a Sezione, Vol. Present. Occas. del Convegno di Stud. I Probl. dei Gd. comprensori irrigui c, 111–123.

D'Agostino, V., 2010. Filtering-retention check dam design in mountain torrents. In: Garcia, C.C., Lenzi, M.A. (Eds.), Check Dams, Morphological Adjustments and Erosion Control in Torrential Streams. Nova Science, New York. Nova Science Publishers, pp. 185–210.

Egashira, S., Ashida, K., 1987. Sediment transport in steep slope flumes. Japan Joint Seminar on Water Resources.

Ellen, S.D., Algus, M.A., Cannon, S.H., Fleming, R.W., Lahr, P.C., Peterson, D.M., Reneau, S.L., 1982. Description and mechanics of soil slip/debris flows in the storm. California. U.S. Geol. Surv. Prof. Pap. 1434, 63–112.

Fischer, J.T., Kowalski, J., Pudasaini, S.P., 2012. Topographic curvature effects in applied avalanche modeling. Cold Reg. Sci. Technol. 74–75, 21–30. https://doi.org/10.1016/j.coldregions.2012.01.005.

Forti, A., 1920. Elementi per la progettazione delle piene catastrofiche nei corsi d'acqua montani. Ann. del Cons. Super. delle Acque 2, 55–74.

Fraccarollo, L., Capart, H., 2002. Riemann wave description of erosional dam-break flows. J. Fluid Mech. 461, 183–228. https://doi.org/10.1017/S0022112002008455.

Fuller, I.C., Large, A.R.G., Charlton, M.E., Heritage, G.L., Milan, D.J., 2003. Reach-scale sediment transfers: an evaluation of two morphological budgeting approaches. Earth Surf. Process. Landforms 28, 889–903. https://doi.org/10.1002/esp.1011.

D'Agostino, V., Pastorello, R., Bettella, F., 2018. Analisi storica degli eventi di piena, analisi idrologica e reologica dei fenomeni di trasporto solido e di massa nel torrente Bigontina a monte dell'abitato di Alverà, in comune di Cortina D'Ampezzo per l'individuazione delle opere idrauliche per la messa in sicurezza di infrastrutture viarie e abitati, Unità Operativa Forestale Est, Belluno, Regione Veneto. (Technical report).

GRASS Development Team, 2020. Geographic Resources Analysis Support System (GRASS) Software, Version 7.8 [WWW Document]. URL http://grass.osgeo.org (accessed 8.1.20).

Gregoretti, C., Degetto, M., Bernard, M., Boreggio, M., 2018. The debris flow occurred at Ru Secco Creek, Venetian Dolomites, on 4 August 2015: analysis of the phenomenon, its characteristics and reproduction by models. Front. Earth Sci. 6, 80. https://doi.org/10.3389/feart.2018.00080.

Gregoretti, C., Stancanelli, L.M., Bernard, M., Boreggio, M., Degetto, M., Lanzoni, S., 2019. Relevance of erosion processes when modelling in-channel gravel debris flows for efficient hazard assessment. J. Hydrol. 568, 575–591. https://doi.org/10.1016/j.jhydrol.2018.10.001.

Griffiths, P.G., Webb, R.H., Melis, T.S., 1997. Initiation of debris flows in tributaries of the Colorado River in Grand Canyon, Arizona, in: 1st International Conference on Debris-Flow Hazards Mitigation, Mechanics, Prediction and Assessment.

Grigorian, S.S., Eglit, M.E., Iakimov, I.L., 1967. New statement and solution of the problem of the motion of snow avalanche. Tr. Vycokogornogo Geofiz. Instituta 12, 104–113.

Grimaldi, S., Petroselli, A., 2015. Do we still need the Rational Formula? An alternative empirical procedure for peak discharge estimation in small and ungauged basins. Hydrol. Sci. J. 60, 67–77. https://doi.org/10.1080/02626667.2014.880546.

Han, Z., Chen, G., Li, Y., Tang, C., Xu, L., He, Y., Huang, X., Wang, W., 2015. Numerical simulation of debris-flow behavior incorporating a dynamic method for estimating the entrainment. Eng. Geol. 190, 52–64. https://doi.org/10.1016/j.enggeo.2015.02.009.

Hungr, O., 1995. A model for the runout analysis of rapid flow slides, debris flows, and avalanches. Can. Geotech. J. 32, 610–623. https://doi.org/10.1139/t95-063.

Hungr, O., Morgan, G.C., Kellerhals, R., 1984. Quantitative analysis of debris torrent hazards for design of remedial measures. Can. Geotech. J. 21, 663–677. https://doi.org/10.1139/t84-073.

Hungr, O., McDougall, S., Bovis, M., 2005. Entrainment of Material by Debris Flows, in: Debris-Flow Hazards and Related Phenomena. Springer, Berlin, Heidelberg, pp. 135–158 https://doi.org/10.1007/3-540-27129-5_7.

Hungr, O., Leroueil, S., Picarelli, L., 2014. The Varnes classification of landslide types, an update. Landslides 11, 167–194. https://doi.org/10.1007/s10346-013-0436-y.

Hutter, K., Svendsen, B., Rickenmann, D., 1994. Debris flow modeling: a review. Contin. Mech. Thermodyn. doi:10.1007/BF01175749

Hutter, K., Svendsen, B., Rickenmann, D., 1996. Debris flow modeling: a review. Contin. Mech. Thermodyn. 23, 93. https://doi.org/10.1016/S0301-9322(97)80255-8.

Iverson, R.M., 1997. The Physics of debris flow. Rev. Geophys. 35, 245–296. https://doi.org/10.1603/033.046.0206.

Iverson, R.M., 2012. Elementary theory of bed-sediment entrainment by debris flows and avalanches. J. Geophys. Res. Earth Surf. 117, 1–17. https://doi.org/10.1029/2011JF002189.

Iverson, R.M., Ouyang, C., 2015. Entrainment of bed material by Earth-surface mass flows: review and reformulation of depth-integrated theory. Rev. Geophys. 53, 27–58. https://doi.org/10.1002/2013RG000447.

Iverson, R.M., Schilling, S.P., Vallance, J.W., 1998. Objective delineation of lahar-inundation hazard zones. Geol. Soc. Am. Bull. 110, 972–984. https://doi.org/10.1130/0016-7606(1998)110<0972:ODOLIH>2.3.CO;2.

Iverson, R.M., Reid, M.E., Logan, M., LaHusen, R.G., Godt, J.W., Griswold, J.P., 2011. Positive feedback and momentum growth during debris-flow entrainment of wet bed sediment. Nat. Geosci. 4, 116–121. https://doi.org/10.1038/ngeo1040.

Jakob, M., Hungr, O., Jakob, D., 2005. Debris-Flow Hazards and Related Phenomena. Springer.

Kattel, P., Khattri, K.B., Pokhrel, P.R., Kafle, J., Tuladhar, B.M., Pudasaini, S.P., 2016. Simulating glacial lake outburst floods with a two-phase mass flow model. Ann. Glaciol. 57, 349–358. https://doi.org/10.3189/2016AoG71A039.

Kean, J.W., McCoy, S.W., Tucker, G.E., Staley, D.M., Coe, J.A., 2013. Runoff-generated debris flows: Observations and modeling of surge initiation, magnitude, and frequency. J. Geophys. Res. Earth Surf. 118, 2190–2207. https://doi.org/10.1002/jgrf.20148.

Kronfellner-Kraus, G., 1984. Extreme Feststofffrachten und Grabenbildungen von Wildbächen [ex- treme sediment loads and erosion of torrents]. Int. Symp. Interpraevent. Villach 109–118.

Marchi, L., Cavalli, M., 2007. Procedures for the documentation of historical debris flows: application to the Chieppena Torrent (Italian Alps). Environ. Manag. 40, 493–503. https://doi.org/10.1007/s00267-006-0288-5.

Marchi, L., D'Agostino, V., 2004. Estimation of debris-flow magnitude in the Eastern Italian Alps. Earth Surf. Process. Landforms 29, 207–220. https://doi.org/10.1002/esp.1027.

Marchi, L., Cavalli, M., Sangati, M., Borga, M., 2009. Hydrometeorological controls and erosive response of an extreme alpine debris flo. Hydrol. Process. 2727, 2714–2727. doi: https://doi.org/10.1002/hyp.

Marra, F., Morin, E., 2015. Use of radar QPE for the derivation of Intensity–Duration–Frequency curves in a range of climatic regimes. J. Hydrol. 531, 427–440. https://doi.org/10.1016/j.jhydrol.2015.08.064.

Marra, F., Morin, E., 2018. Autocorrelation structure of convective rainfall in semiarid-arid climate derived from high-resolution X-Band radar estimates. Atmos. Res. 200, 126–138. https://doi.org/10.1016/j.atmosres.2017.09.020.

Marra, F., Nikolopoulos, E.I., Creutin, J.D., Borga, M., 2014. Radar rainfall estimation for the identification of debris-flow occurrence thresholds. J. Hydrol. 519, 1607–1619. https://doi.org/10.1016/j.jhydrol.2014.09.039.

McDougall, S., Hungr, O., 2005. Dynamic modelling of entrainment in rapid landslides. Can. Geotech. J. 42, 1437–1448. https://doi.org/10.1139/t05-064.

Mergili, M., Pudasaini, S.P., 2020. r.avaflow - the mass flow simulation tool [WWW Document]. URL https://www.avaflow.org (accessed 1.7.20).

Mergili, M., Fischer, J.T., Krenn, J., Pudasaini, S.P., 2017. R.avaflow v1, an advanced open-source computational framework for the propagation and interaction of two-phase mass flows. Geosci. Model Dev. 10, 553–569. https://doi.org/10.5194/gmd-10-553-2017.

Mergili, M., Emmer, A., Juřicová, A., Cochachin, A., Fischer, J.T., Huggel, C., Pudasaini, S.P., 2018. How well can we simulate complex hydro-geomorphic process chains? The 2012 multi-lake outburst flood in the Santa Cruz Valley (Cordillera Blanca, Perú). Earth Surf. Process. Landforms 43, 1373–1389. https://doi.org/10.1002/esp.4318.

Mishra, S.K., Singh, V.P., 2003. Soil Conservation Service Curve Number (SCS-CN) Methodology. Water Science and Technology Library. Springer Netherlands, Dordrecht https://doi.org/10.1007/978-94-017-0147-1.

O'Brien, J.S., 1986. Physical Processes, Rheology and Modeling of Mudflows. Colorado State University.

O'Brien, J.S., Julien, P.Y., Fullerton, W.T., 1993. Two-Dimensional water flood and mudflow simulation. J. Hydraul. Eng. 119, 244–261.

Oliver, M.A., Webster, R., 1990. Kriging: a method of interpolation for geographical information systems. Int. J. Geogr. Inf. Syst. 4, 313–332. https://doi.org/10.1080/02693799008941549.

Pastorello, R., D'Agostino, V., Hürlimann, M., 2020. Debris flow triggering characterization through a comparative analysis among different mountain catchments. Catena 186, 104348. https://doi.org/10.1016/j.catena.2019.104348.

Pirulli, M., Pastor, M., 2012. Numerical study on the entrainment of bed material into rapid landslides. Géotechnique 62, 959–972. https://doi.org/10.1680/geot.10.p.074.

Pitman, E.B., Long, L.E. Le, 2005. A two-fluid model for avalanche and debris flows. Philos. Trans. R. Soc. A Math. Phys. Eng. Sci. 363, 1573–1601. https://doi.org/10.1098/rsta.2005.1596.

Pudasaini, S.P., 2012. A general two-phase debris flow model. J. Geophys. Res. Earth Surf. 117, 1–28. https://doi.org/10.1029/2011JF002186.

Pudasaini, S.P., Fischer, J.T., 2020. A mechanical erosion model for two-phase mass flows. Int. J. Multiph. Flow 132, 1–16. https://doi.org/10.1016/j.ijmultiphaseflow.2020.103416.

Pudasaini, S.P., Mergili, M., 2019. A multi-phase mass flow model. J. Geophys. Res. Earth Surf. 124, 1–23. https://doi.org/10.1029/2019jf005204.

Pudasaini, S.P., Wang, Y., Hutter, K., 2005. Modelling debris flows down general channels. Nat. Hazards Earth Syst. Sci. 5, 799–819. https://doi.org/10.5194/nhess-5-799-2005.

R Core Team, 2020. R: a language and environment for statistical computing [WWW Document]. R Found. Stat. Comput. URL http://www.r-project.org (accessed 8.1.20).

Reid, M.E., Iverson, R.M., Logan, M., Lahusen, R.G., Godt, J.W., Griswold, J.P., 2011. Entrainment of bed sediment by debris flows: Results from large-scale experiments, in: International Conference on Debris-Flow Hazards Mitigation: Mechanics, Prediction, and Assessment, Proceedings. pp. 367–374. doi:10.4408/IJEGE.2011-03.B-042

Rickenmann, D., 2007. Runout prediction methods, in: Springer (Ed.), Debris-Flow Hazards and Related Phenomena. Berlin, pp. 305–324. doi:https://doi.org/10.1007/3-540-27129-5_12

Rickenmann, D., Zimmermann, M., 1993. The 1987 debris flows in Switzerland: documentation and analysis. Geomorphology 8, 175–189. https://doi.org/10.1016/0169-555X(93)90036-2.

Rickenmann, D., Weber, D., Stepanov, B., 2003. Erosion by debris flows in field and laboratory experiments. Int. Conf. Debris-Flow Hazards Mitig. Mech. Predict. Assessment, Proc. 2, 883–894.

Rosatti, G., Begnudelli, L., 2013. Two-dimensional simulation of debris flows over mobile bed: Enhancing the TRENT2D model by using a well-balanced Generalized Roe-type solver. Comput. Fluids 71, 179–195. https://doi.org/10.1016/j.compfluid.2012.10.006.

Sampl, P., Zwinger, T., 2004. Avalanche simulation with SAMOS. Ann. Glaciol. 38, 393–398. https://doi.org/10.3189/172756404781814780.

Savage, S.B., Hutter, K., 1989. The motion of a finite mass of granular material down a rough incline. J. Fluid Mech. 199, 177–215. https://doi.org/10.1017/S0022112089000340.

Takahashi, T., 2000. Initiation and flow of various types of debris-flow. Debris-Flow Hazards Mitigation: Mechanics, Prediction, and Assessment, pp. 15–25.

Takahashi, T., 2007. Debris Flow: Mechanics, Prediction and Countermeasures.

Takahashi, T., Das, D., 2014. Debris Flow: Mechanics, Prediction and Countermeasures, 2nd editio. ed. CRC Press, Balkema.

Takahashi, T., Kuang, S.F., 1986. Formation of debris flow on varied slope bed. Disaster Prev. Res. Inst. Annu. 29, 343–359.

Takahashi, T., Nakagawa, H., Harada, T., Yamashiki, Y., 1992. Routing Debris Flows with Particle Segregation. J. Hydraul. Eng. 118, 1490–1507. https://doi.org/10.1061/(ASCE)0733-9429(1992)118:11(1490.

Voellmy, A., 1955. Über die Zerstörungskraft von Lawinen. Schweizerische Bauzeitung 73, 159–165. https://doi.org/10.2746/042516407X182811.